Coseismic subsidence in the 1700 great Cascadia earthquake: Coastal estimates versus elastic dislocation models

Lucinda J. Leonard[†]
School of Earth and Ocean Sciences, University of Victoria, Post Office Box 3055 STN CSC, Victoria, British Columbia V8W 3P6, Canada and *Geological Survey of Canada, Pacific Geoscience Centre, 9860 West Saanich Road, Sidney, British Columbia V8L 4B2, Canada*

Roy D. Hyndman[‡]
Geological Survey of Canada, Pacific Geoscience Centre, 9860 West Saanich Road, Sidney, British Columbia V8L 4B2, Canada, and *School of Earth and Ocean Sciences, University of Victoria, Post Office Box 3055 STN CSC, Victoria, British Columbia V8W 3P6, Canada*

Stéphane Mazzotti[§]
Geological Survey of Canada, Pacific Geoscience Centre, 9860 West Saanich Road, Sidney, British Columbia V8L 4B2, Canada

ABSTRACT

Seismic hazard assessments for a Cascadia subduction zone earthquake are largely based on the rupture area predictions of dislocation models constrained by geodetic and geothermal data; this paper tests the consistency of the models for the 1700 great Cascadia earthquake with compiled coastal coseismic subsidence as estimated from paleoelevation studies. Coastal estimates have large uncertainties but show a consistent pattern. Greatest coseismic subsidence (~1–2 m) occurred in northern Oregon/southern Washington; subsidence elsewhere was ~0–1 m. Elastic dislocation models constrained by interseismic geodetic and thermal data are used to predict the coseismic subsidence for two likely strain accumulation periods of (i) 800 and (ii) 550 yr of plate convergence and for uniform megathrust slip of 10, 20, 30, and 50 m. The former two models provide a better and equally good fit; predicted subsidence is in broad agreement with marsh estimates. Discrepancies exist, however, at the ends of the subduction zone. In the south, misfit may be due to breakup of the Gorda plate. The discrepancy in the north may be explained if the 1700 event released only part of the accumulated strain there, consistent with long-term net uplift in excess of eustatic sea-level rise. The coseismic slip magnitude, estimated by comparing uniform slip model predictions with marsh coseismic subsidence estimates, is consistent with the M 9 earthquake indicated by Japanese tsunami records. The coseismic slip was greatest in northern Oregon/southern Washington, declining to the north and south.

Keywords: Cascadia subduction zone, earthquakes, modeling, Holocene, estuaries, paleoseismology.

INTRODUCTION

Despite the lack of great megathrust earthquakes at the Cascadia subduction zone (Fig. 1) in the last 200 yr, their occurrence approximately every 500 yr is supported by several lines of evidence. Japanese records of wave heights from a far-field tsunami in January 1700 are consistent with an M 9 earthquake on the Cascadia megathrust (Satake et al., 1996). This is compatible with Native American oral records from Cascadia (Ludwin, 2002) and with coastal subsidence evidenced by buried soils and submerged trees where the time of submergence can in some cases be dated to lie between the 1699 and 1700 growing seasons (Yamaguchi et al., 1997; Jacoby et al., 1997).

Geodetic measurements (e.g., Savage and Lisowski, 1991; Dragert et al., 1994; Mitchell et al., 1994; Hyndman and Wang, 1995; McCaffrey et al., 2000; Miller et al., 2001) indicate that the Cascadia subduction thrust is presently locked and that interseismic strain accumulation is causing uplift and shortening along much of the coast. Figure 2 shows the interseismic and coseismic deformation expected with such a subduction thrust fault. Close to the deformation front, there is interseismic subsidence and coseismic uplift, whereas farther landward, coinciding with much of the Cascadia coast, a pattern of interseismic uplift and coseismic subsidence prevails. Such patterns of interseismic and inverse coseismic vertical motions have been observed at other subduction zones that have experienced historical great earthquakes, including Chile (Plafker and Savage, 1970), Alaska (e.g., Plafker, 1972), and southwestern Japan (e.g., Thatcher, 1984; Savage and Thatcher, 1992).

The determination of the amount of coseismic slip, and hence subsidence, in the 1700 and previous events is crucial to our understanding of seismic hazard in the region. Current hazard assessments for great earthquakes are largely based on the predictions of elastic dislocation models, which are constrained by recent geodetic strain measurements and by thermal estimates. The main objective of this study is to compare the magnitude of coseismic subsidence estimated from coastal marsh studies for the 1700 event with that predicted by elastic dislocation models. The need for this comparison has been stressed previously (Flück et al., 1997; Long and Shennan, 1998). The coastal marsh data perpendicular to the margin (east-west) are too limited to uniquely

[†]E-mail: lucindal@uvic.ca.
[‡]E-mail: rhyndman@nrcan.gc.ca.
[§]E-mail: smazzotti@nrcan.gc.ca.

GSA Bulletin; May/June 2004; v. 116; no. 5/6; p. 655–670; doi: 10.1130/B25369.1; 14 figures; 1 table; Data Repository item 2004076.

For permission to copy, contact editing@geosociety.org
© 2004 Geological Society of America

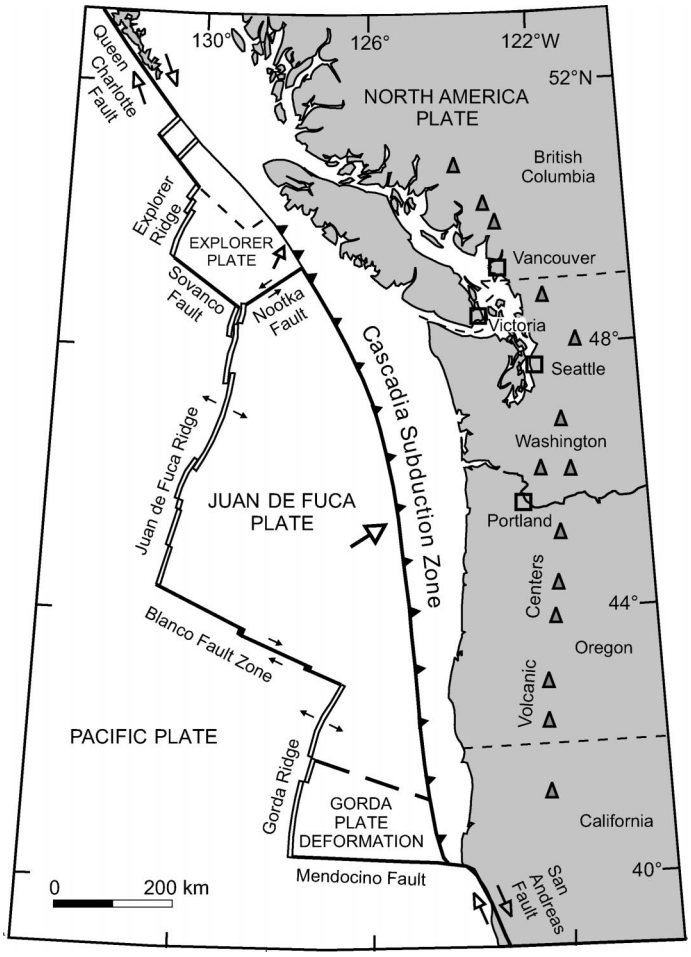

Figure 1. Plate tectonic setting of the Cascadia subduction zone.

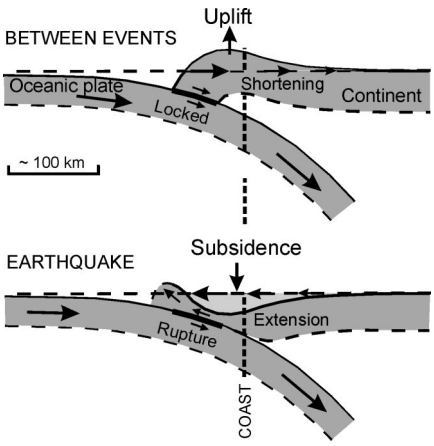

Figure 2. Pattern of interseismic and coseismic deformation expected with a subduction thrust fault (modified from Dragert et al., 1994). Much of Cascadia coast is currently undergoing interseismic uplift; during a great earthquake this area is subject to coseismic subsidence.

constrain the rupture area. However, the coastal data do provide a strong constraint to the rupture area, especially the critical landward limit. The coastal subsidence data for great Cascadia earthquakes prior to the 1700 event are very limited but indicate that the magnitude of subsidence has varied (e.g., Peterson et al., 1997); future studies may allow comparisons similar to our work on the 1700 earthquake.

COSEISMIC SUBSIDENCE IN MEGATHRUST EARTHQUAKES

Coastal coseismic subsidence and uplift in historical subduction zone earthquakes have been documented in Alaska, Chile, and Japan. In the case of the 1960 Chile and 1964 Alaska great earthquakes, coseismic subsidence converted some vegetated coastal lowlands to barren estuarine mudflats (e.g., Plafker and Savage, 1970; Ovenshine et al., 1976). At the head of Cook Inlet near Portage, Alaska, aggradation and uplift have since permitted the reestablishment of lowland trees and shrubs (Ovenshine et al., 1976; Brown et al., 1977; Atwater et al., 2001). Therefore, in a stratigraphic sequence, a layer of peat overlain by intertidal mud (''peat-mud couplet'') that grades upward into another peat layer may represent a cycle of coseismic subsidence and interseismic shoaling (Atwater, 1987) as shown in Figure 3. Peat-mud couplets have also been cited as evidence of ancient subduction earthquakes in Chile and Alaska (e.g., Wright and Mella, 1963; Ovenshine et al., 1976; Combellick, 1986).

Atwater (1987) was the first to describe buried soils at Cascadia in detail and attribute them to past subduction megathrust earthquakes. They have since been found to occur at many estuaries along the coast in northern California, Oregon, Washington, and southern Vancouver Island, British Columbia (Fig. 4). Figure 5 shows a typical peat-mud couplet in Cascadia, where the peat is capped by tsunami-deposited sand. These sequences, as in Chile and Alaska, have also been attributed to ancient subduction earthquakes.

However, peat-mud couplets are not uniquely a product of large earthquakes; similar stratigraphic sequences are observed at mid-latitude passive margin coasts and may be caused by a range of local and regional aseismic processes that result in relative sea-level changes (e.g., Nelson et al., 1996a). Thus, there must be criteria to distinguish peat-mud couplets that result from great earthquake subsidence from those that are produced by other processes. The 1700 buried soil fulfills the criteria established by Nelson et al. (1996a): (1) subsidence was sudden, as evidenced by the preservation of growth position macrofossils; (2) it amounted to at least 0.5 m along the majority of the coast; (3) lasting submergence is shown by a long-term switch to lower intertidal zones above the 1700 horizon; (4) the 1700 soil is widely correlated; and (5) it is often covered by a laminated sandy deposit (e.g., Fig. 5) inferred as the product of a tsunami, generated in the event, that rushed into the subsided coastal area.

There are two methods available to determine the coseismic subsidence from coastal marshes (described in detail in sections below): (1) a technique that finds, by comparison with elevations of the different zones of the modern marsh, the paleoelevation difference between the 1700 horizon and overlying sediments, (2) the depth interval between the modern marsh top and the buried marsh, corrected for global sea-level change, postglacial rebound, and interseismic land uplift. Method 1 and its results, which are primarily a com-

pilation of previously published work, are presented first. We then describe our elastic dislocation models and compare the model predictions of subsidence with the results of method 1. Finally, we discuss method 2 and its results, which are original to this paper.

METHOD 1: ESTIMATING COSEISMIC SUBSIDENCE USING INTERTIDAL ELEVATION INDICATORS ABOVE AND BELOW BURIED MARSH TOP

The magnitude of coseismic subsidence is the difference in paleoelevation between the 1700 marsh top horizon and the sediments that either directly overlie it or that overlie an intervening tsunami sand cap; in the case of the latter, coseismic subsidence amounts to the thickness of the sand deposit added to the paleoelevation difference. Such a definition assumes that (1) the overlying sediment records the time immediately after the earthquake (i.e., prior to any large postseismic deformation), and (2) the sediments are unaffected by compaction or other subsequent disturbance (discussed below).

Paleoelevation is determined by calibration of elevation indicators in the buried sediment with the depth indicators in the zones of the modern marsh surface. Modern intertidal elevational zones may be defined by the distribution of: (1) organic content, (2) vascular plants, (3) foraminiferal assemblages, (4) diatom assemblages, and (5) pollen assemblages. Although the distribution of estuarine organisms is controlled by many biologic and ecologic factors, most of these are directly related to elevation relative to average sea level (e.g., Frey and Basan, 1985; Jennings and Nelson, 1992); it is primarily the amount of subaerial exposure that limits organisms to a particular elevation range (Scott and Medioli, 1980).

In this study we review and analyze published reports on Cascadia marsh subsidence. In some cases we have revised the published subsidence in an effort to use consistent methods along the whole margin. We have also added subsidence estimates to the database based on our interpretation of published stratigraphic and sedimentological data.

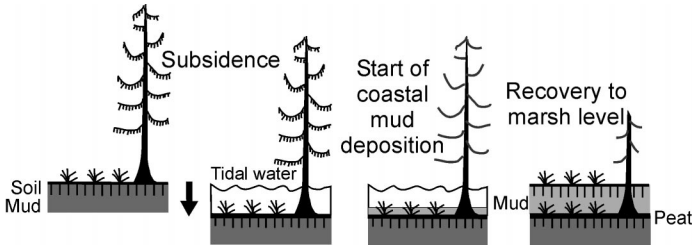

Figure 3. Formation of peat-mud couplets resulting from coseismic subsidence during megathrust earthquakes (modified from Atwater et al., 1995).

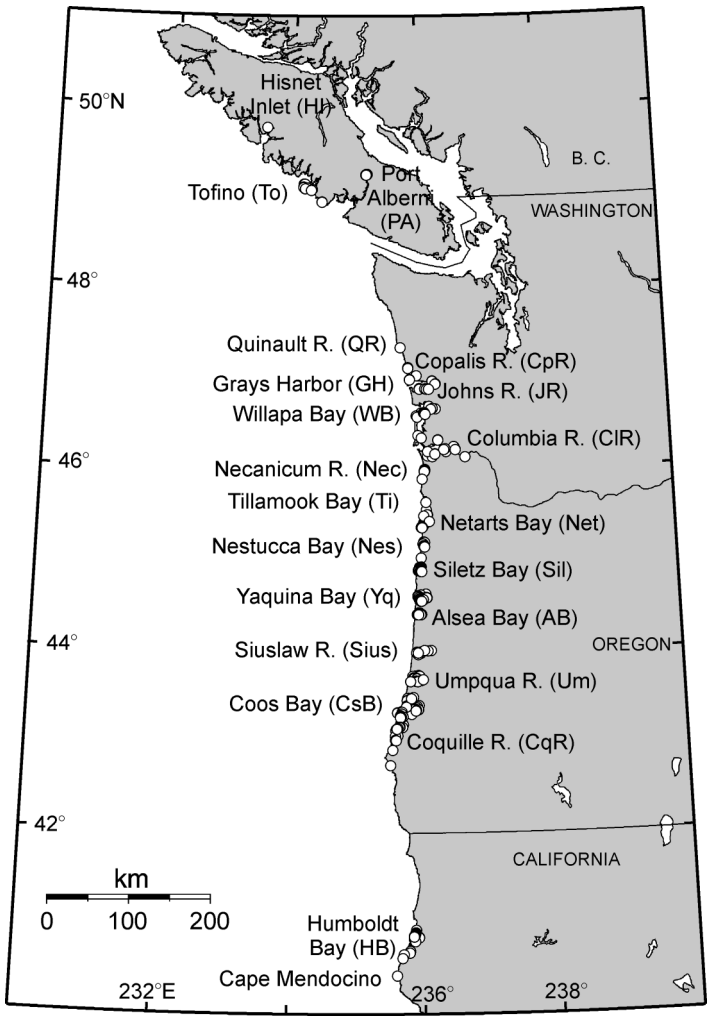

Figure 4. Location of Cascadia estuaries from which subsidence data have been extracted. Open circles mark data sites.

Survey of Modern Marsh

Ideally, the modern marsh reference sites are surveyed in close proximity to the site of fossil data collection; this was done in the studies of Darienzo and Peterson (1990), Hemphill-Haley (1995b), Guilbault et al. (1996), Shennan et al. (1996, 1998), Barnett (1997), Peterson et al. (1997), and Hughes et al. (2002). In estuaries where no modern survey has been done, we compare the fossil data to surveys of nearby estuaries, generally combining the data from several localities to reduce miscorrelation due to site differences. Averaging reference site data results in an increase in the calculated errors of subsidence. A typical modern survey is carried out as follows. One or more surface transects of the modern marsh from the forest edge to the water are sampled at short intervals, for example, at every 10 cm change in elevation; relative elevations are tied into local benchmarks to give absolute elevation with respect to tide level. A number of intertidal zones defined by

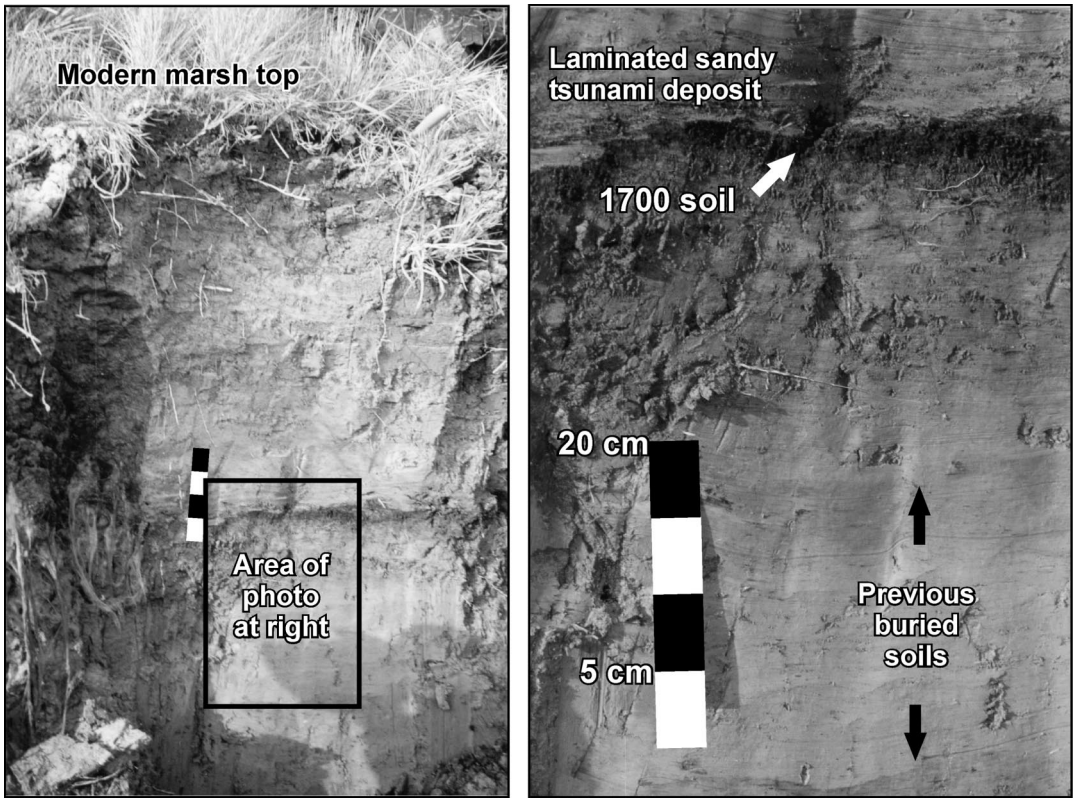

Figure 5. Buried soil from 1700, as exposed in cutbank section of Niawiakum River, Willapa Bay, Washington. Peat from 1700 is overlain by sandy layers interpreted to have been deposited by tsunami coincident with earthquake; sand is, in turn, overlain by intertidal mud, grading up to present marsh surface. Previous megathrust earthquakes are suggested by older buried soils below 1700 horizon. (Photo by author.)

elevation can be determined from analysis of surface and near-surface sediment. Sampling methods and processing are described for analysis of foraminifera by Guilbault et al. (1995), analysis of diatoms by Nelson and Kashima (1993) and Hemphill-Haley (1995a), and analysis of pollen by Hughes et al. (2002).

Organic Content and Plant Macrofossils

Organic content of estuarine sediment generally increases with elevation in the intertidal zone (e.g., Peterson and Darienzo, 1991). Modern Cascadia marshes generally exhibit a continuous vertical transition from mud at low elevations through rooted mud, peaty mud and muddy peat, to peat at higher elevations (for definitions see Peterson and Darienzo, 1991, p. 5). The elevational limits of each of these modern zones may be compared with the buried sediment types to allow paleoelevation to be estimated to a first order. Organic content is estimated visually or by loss on ignition. However, because relative peat development varies considerably among sites, the zoning may not be robust, and estimates based on this property alone are found to be less reliable than those based on fossil assemblages (Nelson et al., 1996a).

Plant macrofossils provide valuable clues to the paleoelevation of buried sediment, although often, few, if any, are preserved. An indicator species in the buried marsh is taken to represent a paleoelevation within the elevation range of that species in the modern marsh; the narrower that modern range, the more precise the paleoelevation estimate. For example: (1) spruce trees will grow no lower than the forest edge; (2) typical high marsh plants are *Potentilla*, *Grindelia*, and *Juncus*; (3) *Salicornia*, *Distichlis*, and *Triglochin* characterize the low marsh; (4) *Triglochin*, *Carex*, and *Scirpus* may colonize the upper tidal flats (e.g., Peterson et al., 1997).

Microfossils: Statistical Methods

At Cascadia, pollen data have been used in only one detailed study: coseismic subsidence was estimated for Tofino, Vancouver Island, by Hughes et al. (2002). Zoning of modern pollen data is achieved by classification with optimal splitting. Determination of indicator taxa (pollen that are good indicators of elevation) and analogue matching between surface and fossil pollen samples allow the development of a transfer function calibration of fossil pollen samples to elevation (for details, see Hughes et al., 2002).

Elsewhere, marine microfossils usually provide the most precise paleoelevation estimates. In foraminiferal and diatom studies, Q-mode factor analysis may be used to cluster the modern data into groups defined by elevation (for details of statistics, see Hemphill-Haley, 1992, 1995a; Guilbault et al., 1995, 1996). Paleoelevation of subsurface horizons is calculated by applying transfer functions (derived from the factor analysis) to factored fossil data. Discriminant function analysis (e.g., Jennings and Nelson, 1992; Nelson and Kashima, 1993; Nelson et al., 1996b) determines how well the modern data are grouped, that is, how statistically distinct the selected zones are. Discriminant functions derived from the modern data are applied to the fossil data for paleoelevation determination. Visual comparison of fossil and modern data usually

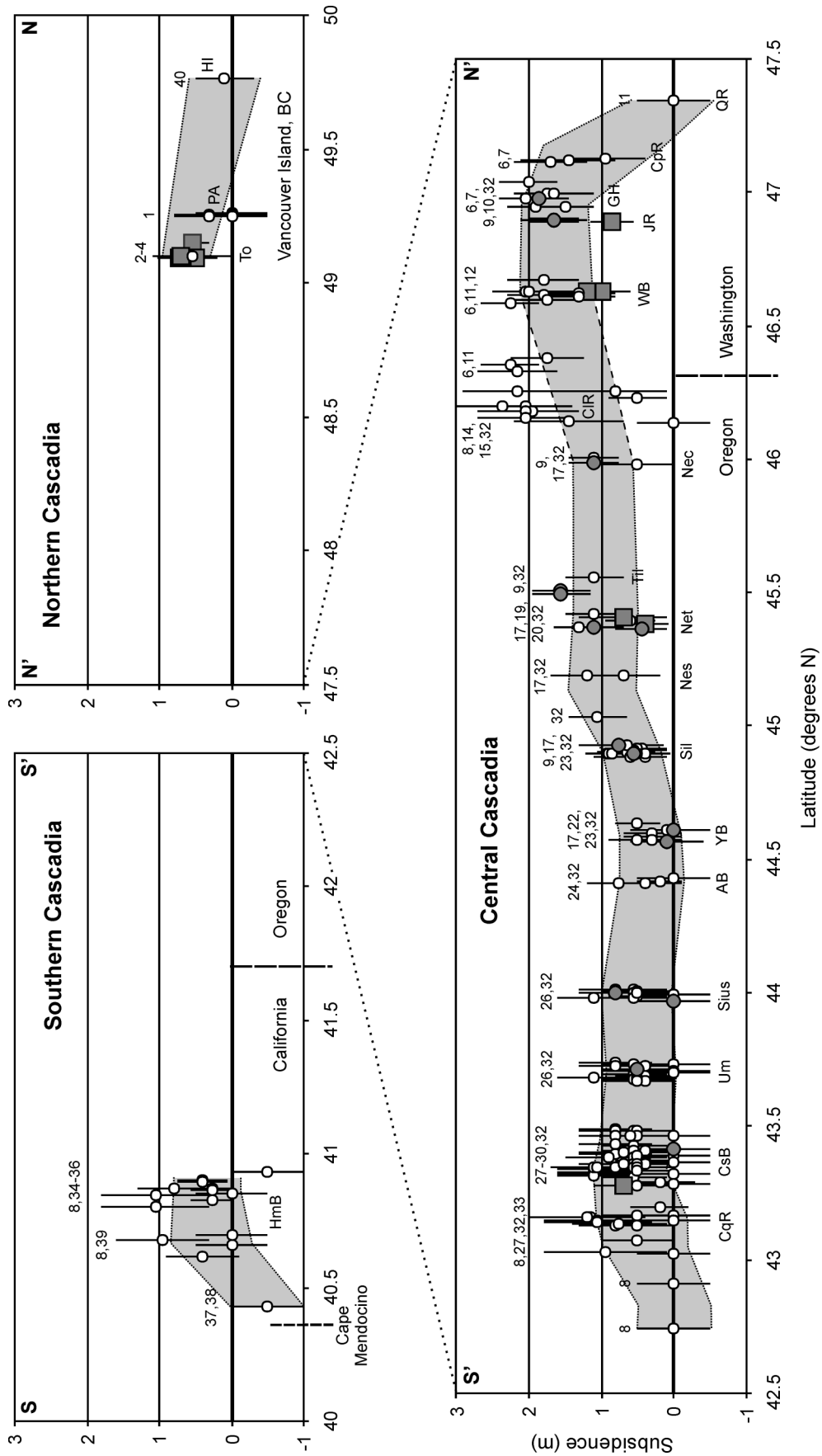

Figure 6. Compilation of coseismic subsidence estimates made using method 1, plotted against latitude. Individual error bars represent uncertainty due to range of possible paleoelevations above and below 1700 horizon. Gray shading represents weighted mean plus or minus weighted standard deviation of groups of points; Columbia River and Port Alberni data are excluded from this shading, the former due to unreliability as discussed in text, the latter due to location significantly inland. Gray squares are estimates made via detailed microfossil studies; gray circles represent estimates made using organic content and relative percentage of freshwater/brackish diatoms plus or minus plant macrofossils; open circles are estimates made using organic content plus or minus plant macrofossils. Locations and abbreviations are shown in Figure 4. Numbers above data points reference data sources (see Table 1).

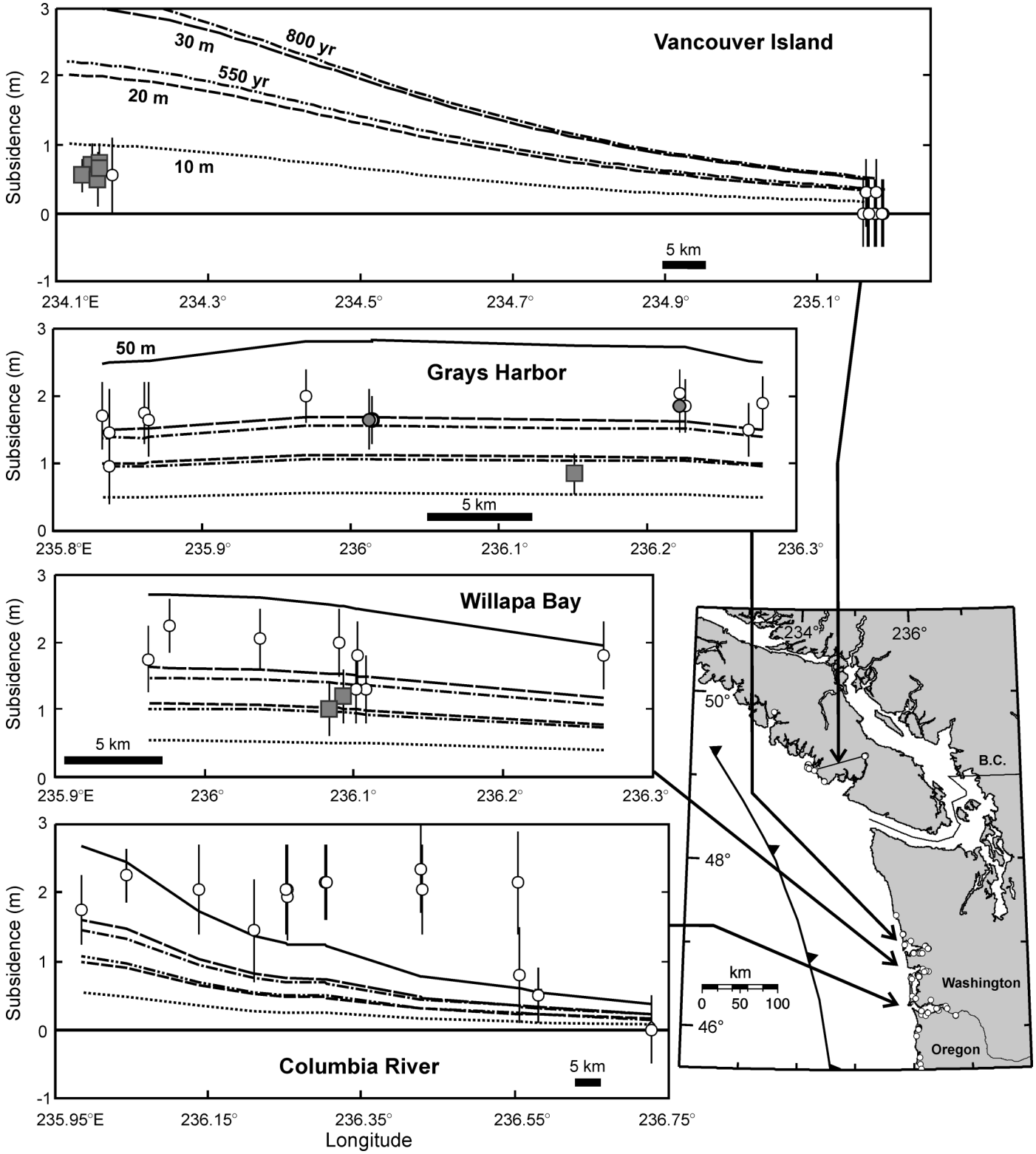

Figure 7. Transverse sections of Cascadia coastal subsidence data plotted against longitude, in comparison with subsidence predictions (for same sites) of elastic dislocation models described in text. Error bars and symbols as explained in Figure 6. Notches apparent in model curves are due to north-south variations in site locations.

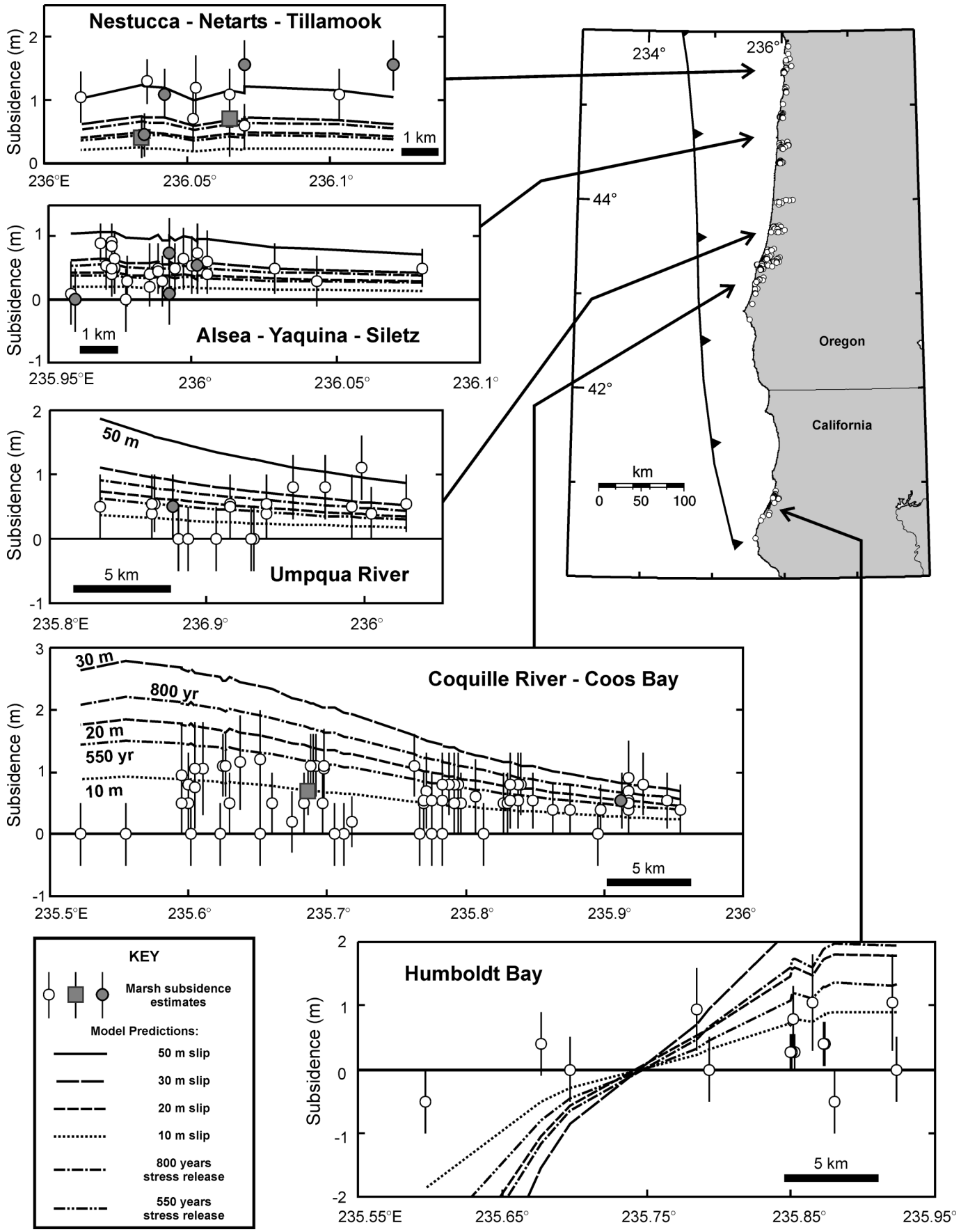

Figure 7. (*Continued.*)

TABLE 1. SUMMARY OF ESTIMATED 1700 CASCADIA COSEISMIC SUBSIDENCE

Marsh location	Average depth of 1700 soil (m)	Range of estimated subsidence (m)	Coseismic subsidence: mean ± standard deviation (m)	Data sources
Port Alberni	0.46	0 ± 0.5 to 0.3 ± 0.5	0.07 ± 0.13	1
Tofino	0.28	0.5 ± 0.3 to 0.72 ± 0.3	0.62 ± 0.09	2–5
Copalis R.	1.18	0.95 ± 0.55 to 1.7 ± 0.5	1.37 ± 0.38	6, 7
Grays Harbor	0.59	0.85 ± 0.3 to 2.05 ± 0.35	1.7 ± 0.31	6, 8–10
Willapa Bay	0.83	1 ± 0.4 to 2.25 ± 0.4	1.7 ± 0.42	6,11–13
Columbia R.	1.00	0 ± 0.5 to 2.35 ± 0.65	1.67 ± 0.75	6, 8,14–16
Necanicum R.	0.61	0.5 ± 0.5 to 1.1 ± 0.35	0.9 ± 0.35	8, 9, 17, 18
Tillamook Bay	0.51	1.1 ± 0.4 to 1.55 ± 0.4	1.4 ± 0.26	8,15
Netarts Bay	0.61	0.4 ± 0.32 to 1.1 ± 0.4	0.81 ± 0.36	8,17,19–21
Nestucca Bay	0.69	0.7 ± 0.5 to 1.2 ± 0.5	0.95 ± 0.35	8,17
Siletz Bay	0.60	0.4 ± 0.35 to 0.9 ± 0.3	0.58 ± 0.15	8, 9, 17, 19
Yaquina Bay	0.58	0 ± 0.5 to 0.5 ± 0.4	0.29 ± 0.19	8, 17, 22, 23
Alsea Bay	0.51	0 ± 0.5 to 0.75 ± 0.45	0.34 ± 0.32	8, 17, 24, 25
Siuslaw	0.88	0 ± 0.5 to 1.1 ± 0.5	0.53 ± 0.31	8,26
Umpqua	0.95	0 ± 0.5 to 1.1 ± 0.5	0.46 ± 0.31	8,26
Coos Bay	0.72	0 ± 0.5 to 1.1 ± 0.6	0.61 ± 0.32	8, 26–31
Coquille	0.77	0 ± 0.5 to 1.2 ± 0.8	0.51 ± 0.45	8, 27, 32, 33
Humboldt Bay	1.10	0 ± 0.5 to 1.05 ± 0.75	0.44 ± 0.37	34–36

Notes: Data sources: 1—Clague and Bobrowsky (1994b), 2—Hughes et al. (2002), 3—Guilbault et al. (1996), 4—Clague and Bobrowsky (1994a), 5—Guilbault et al. (1995), 6—Atwater (1988), 7—Atwater (1992), 8—Peterson et al. (1997), 9—Barnett (1997), 10—Shennan et al. (1996), 11—Peterson et al. (2000), 12—Hemphill-Haley (1995b), 13—Atwater and Hemphill-Haley (1997), 14—Atwater (1994), 15—Peterson et al. (1993), 16—Peterson and Madin (1997), 17—Darienzo (1991), 18—Gallaway et al. (1992), 19—Shennan et al. (1998), 20—Darienzo and Peterson (1990), 21—Peterson and Darienzo (1988), 22—Peterson and Priest (1995), 23—Peterson et al. (1996), 24—Peterson and Darienzo (1996), 25—Peterson and Darienzo (1991), 26—Briggs (1994), 27—Nelson (1992), 28—Nelson et al. (1996b), 29—Peterson and Darienzo (1989), 30—Darienzo and Peterson (1995), 31—Nelson et al. (1998), 32—Briggs and Peterson (1993), 33—Witter et al. (1997), 34—Vick (1988), 35—Carver and Burke (1989), 36—Jacoby et al. (1995). Additional data sources for Figures 6 and 13: 37—Carver et al. (1994), 38—Merritts (1996), 39—Li (1992), 40—Hutchinson et al. (2000).

yields paleoelevation estimates that are very comparable to those derived from statistical methods (e.g., Guilbault et al., 1995).

Sources of Error

The correlation of a buried sediment horizon with a modern intertidal zone elevation is a relatively precise way of determining its paleoelevation; however, the accuracy of the methods described above depends on a number of factors:

(1) The width and thus elevation range of intertidal zones are functions of the local tidal range; intertidal zones at Cascadia are typically broad and have gradational boundaries (e.g., Jennings and Nelson, 1992; Hemphill-Haley, 1995a). These factors reduce the resolution of coseismic subsidence estimates. Use of a combination of elevation indicators that differ in their zonation narrows the acceptable paleoelevation range.

(2) The elevations of upland and mudflat zones are only defined at the lower and upper ends, respectively. Thus, in a stratigraphic sequence, only the minimum change to or from either of these zones can be estimated with useful accuracy (e.g., Jennings and Nelson, 1992).

(3) A modern marsh survey should be carried out in as close proximity as possible to the fossil sample site so that it represents the best possible calibration analogue. Neighboring estuaries may have different tidal ranges, and within an estuary, local site differences such as the presence of streams may increase error (e.g., Guilbault et al., 1996). At most Cascadia estuaries it is probably safe to assume that tidal conditions within an individual estuary have not changed significantly in the last 300 yr (e.g., Peterson and Darienzo, 1991; Nelson et al., 1996a). However, there is no modern analogue at Cascadia for the sediments immediately above the 1700 horizon and tsunami sand; the estuarine environment in the aftermath of coseismic subsidence is little understood (e.g., Shennan et al., 1998; Hughes et al., 2002).

(4) If the sediment section was affected by compaction due to shaking at the time of the earthquake, coseismic subsidence will be overestimated. Compaction accounted for a significant proportion of subsidence in the 1964 Alaska earthquake (0.8 m of 2.4 m subsidence in the Portage area) (Ovenshine et al., 1976). However, the Portage area is underlain by ~300 m of unconsolidated sediment, and compaction does not appear to have played a significant role in subsidence at Cascadia, where unconsolidated sediments are thin. The 1700 soil can be traced in outcrop onto indurated Pleistocene deposits at the Copalis River and Willapa Bay, Washington (Atwater, 1987, 1992; Atwater and Hemphill-Haley, 1997); at Tofino, Vancouver Island, the Holocene sequence (< 2 m thick) overlies compact glaciomarine clay and shows no systematic difference in unit thickness for sites close to bedrock and those further away with thicker recent sediments (Clague and Bobrowsky, 1994a; Guilbault et al., 1995). In cores from Alsea Bay, Oregon, Peterson and Darienzo (1991) found relatively small changes in bulk density downcore, suggesting that compaction has not been a major factor.

(5) Another concern is whether the sediments overlying the 1700 horizon were deposited quickly enough that they predate significant postseismic deformation associated with deep creep on the fault or viscoelastic rebound of the mantle. The postseismic vertical deformation could produce either uplift or extra subsidence in the zone of coseismic subsidence. Postseismic uplift of up to 0.55 m in one area had occurred in 12 yr following the 1964 Alaska earthquake (Brown et al., 1977). The buried peat near Tofino is overlain by an undisturbed layer of tsunami sand; the fact that this was not washed away while exposed in the intertidal zone suggests that sedimentation resumed almost immediately after the 1700 quake (Guilbault et al., 1996). At Tofino, paleoelevation studies (pollen and foraminifera) indicate that the sediment between 1 and 7 cm above the tsunami sand represents 40 cm of uplift; the difference (34 ± 30 cm) is attributed to postseismic rebound (Guilbault et al., 1996; Hughes et al., 2002). Higher than 7 cm, sedimentation has kept pace with elevation change (20 cm uplift in 17 cm sediment), suggesting that postseismic rebound had practically ceased after 7 cm of sedimentation. Guilbault et al. (1996) suggest that this sediment thickness represents a few to several decades. Discriminating the rate of sedimentation in interseismic sediments has yet to be accomplished (Shennan et al., 1998).

An important question is whether populations had time to colonize the post-1700 sediments before much rebound occurred and therefore to record the full amount of coseismic subsidence. Diatom populations can establish themselves within days to weeks in shallow water, and therefore fossil assemblages in post-1700 sediments should record mainly coseismic subsidence (Hemphill-Haley, 1995b).

(6) There may be a bias in the microfossil record due to differential preservation or transport that increases the error of coseismic subsidence estimates. For example, finely silicified diatom species such as *Gyrosigma* spp. are vulnerable to dissolution, whereas the marine-brackish water benthic species *Paralia*

sulcata is very resistant. Because the latter forms long chains that are easily entrained into the plankton, its abundance is readily enhanced in estuarine deposits as allochthonous (transported) valves (Hemphill-Haley, 1995b).

Cascadia Coseismic Subsidence Estimates

A compilation of coseismic subsidence estimates (Table DR1; summary in Table 1) is shown plotted against latitude in Figure 6 and against longitude in Figure 7.[1] There are two large gaps in data along the Cascadia coast, one extending between central Washington and central Vancouver Island and the other between southern Oregon (Coquille) and Humboldt Bay, northern California. These areas lack large tidal marshes (Peterson et al., 1997). Some of the compiled estimates have been published while others are interpretations of published core logs or reinterpretations of published estimates based on comparison with modern surveys of intertidal zones in nearby estuaries, for example, as described by Peterson et al. (1997) for a number of Washington and Oregon estuaries, Shennan et al. (1998) for Netarts Bay, Oregon, Jennings and Nelson (1992) and Nelson and Kashima (1993) for Coos Bay and Siuslaw River, Oregon, and Shennan et al. (1996) for Johns River, Washington.

The plotted uncertainty on the coseismic subsidence estimates (± 0.25 to 0.8 m; Figs. 6 and 7) results mainly from the width of intertidal zones, which control the size of the paleoelevation ranges used to calculate coseismic subsidence. For sites where the modern marsh has not been surveyed, uncertainty is increased as previously described. Errors are greater in the event that unrecognized compaction, postseismic rebound, or bias in the fossil record, as discussed above, were significant.

ELASTIC DISLOCATION MODEL

The model coseismic subsidence predictions are from the three-dimensional elastic dislocation fault model developed for the Cascadia subduction zone by Flück et al. (1997). The model is based on the point source solution by Okada (1985); deformation at each location on the Earth's surface is calculated by numerical integration of point source dislocations over the fault plane (details in Flück et al., 1997). The model assumes elastic behavior; that is, all of the strain accumulated over the earthquake cycle is released in the earthquake. It also assumes that strain accumulation occurs at the present rate throughout the earthquake cycle. The geometry of the subduction thrust fault is constrained by Benioff-Wadati seismicity, seismic reflection, seismic refraction, seismic tomography, and teleseismic waveform analysis (Hyndman and Wang, 1995; Flück et al., 1997). The thrust fault consists of a locked zone and a transition zone (Fig. 8). The entire locked zone ruptures in an earthquake and is locked between events; its updip and downdip limits may be thermally controlled (e.g., Hyndman and Wang, 1993, 1995). In the simple model for the transition zone, fault rupture is assumed to decrease linearly downdip to zero; continuous aseismic slip is assumed to occur downdip of this zone.

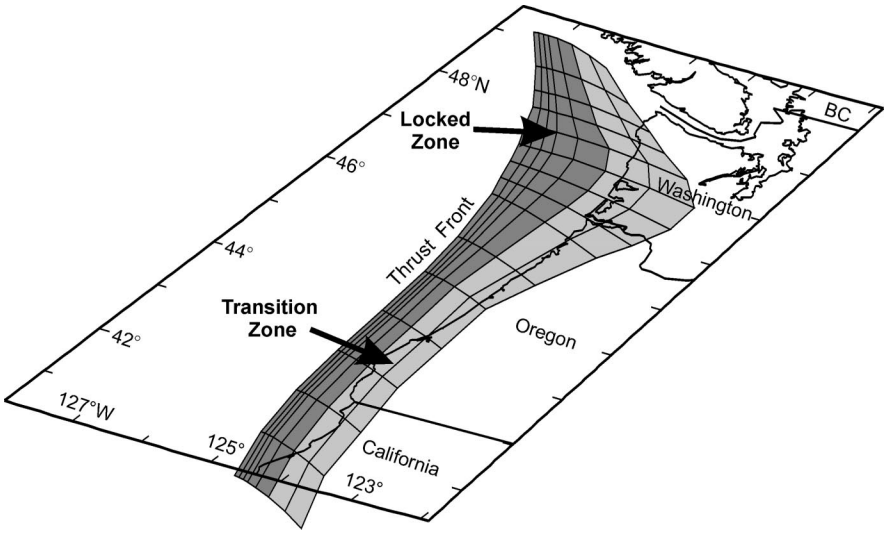

Figure 8. Locked and transition zones of Cascadia megathrust (based on thermal constraints and geodetic data) used in elastic dislocation model (after Flück et al., 1997).

The model is constrained by geodetic data including repeated leveling, repeated gravity, tide-gauge data, triangulation-trilateration laser ranging, and Global Positioning System data (cf., references in Hyndman and Wang [1995] and Flück et al. [1997]). Some minor model refinements have been suggested based on recent horizontal GPS data (McCaffrey et al., 2000; Miller et al., 2001; Svarc et al., 2002; Mazzotti et al., 2002), but deformation of the forearc makes horizontal data more complex compared to the mainly vertical data used by Flück et al. (1997). In this study, we use an updated Flück et al. (1997) model, but the coastal data may be readily compared to other model variations. The convergence direction and rate between the Juan de Fuca (and Gorda) and North America plates vary along the margin due to clockwise rotation of the Juan de Fuca plate with respect to North America (Wilson, 1993). The convergence increases continuously northward from 27 mm/yr toward 042° at the southern end of the subduction zone to 45 mm/yr toward 056° at the northern end. More margin-normal and higher rates of convergence result in greater coseismic slip, and thus it is critical to incorporate these variations into the model. In our model we have ignored the small effect of the motion of the Cascadia forearc relative to North America.

MODEL PREDICTIONS AND COMPARISON WITH COASTAL MARSH ESTIMATES

The elastic dislocation model is used in two ways to predict the coseismic subsidence that occurred in 1700. Our first approach is to predict the amount of subsidence expected upon release of all the strain built up as a result of convergence over a particular time period. We use strain buildup for two different time intervals. The first uses the ~800 yr (600–1000) between the previous megathrust earthquake and the 1700 event (Atwater and Hemphill-Haley, 1997), and the second uses an average recurrence interval of 550 yr (500–540 yr over the last 3500 yr from marshes, Atwater and Hemphill-Haley [1997]; 590 yr over 7770 yr from deep sea turbidites, Adams [1990]). For 800 yr of convergence, the slip increases from 21.6 m in the south to 36 m in the north, and

[1]GSA Data Repository item 2004076, depth of 1700 horizon and estimated 1700 Cascadia coseismic subsidence, is available on the Web at http://www.geosociety.org/pubs/ft2004.htm. Requests may also be sent to editing@geosociety.org.

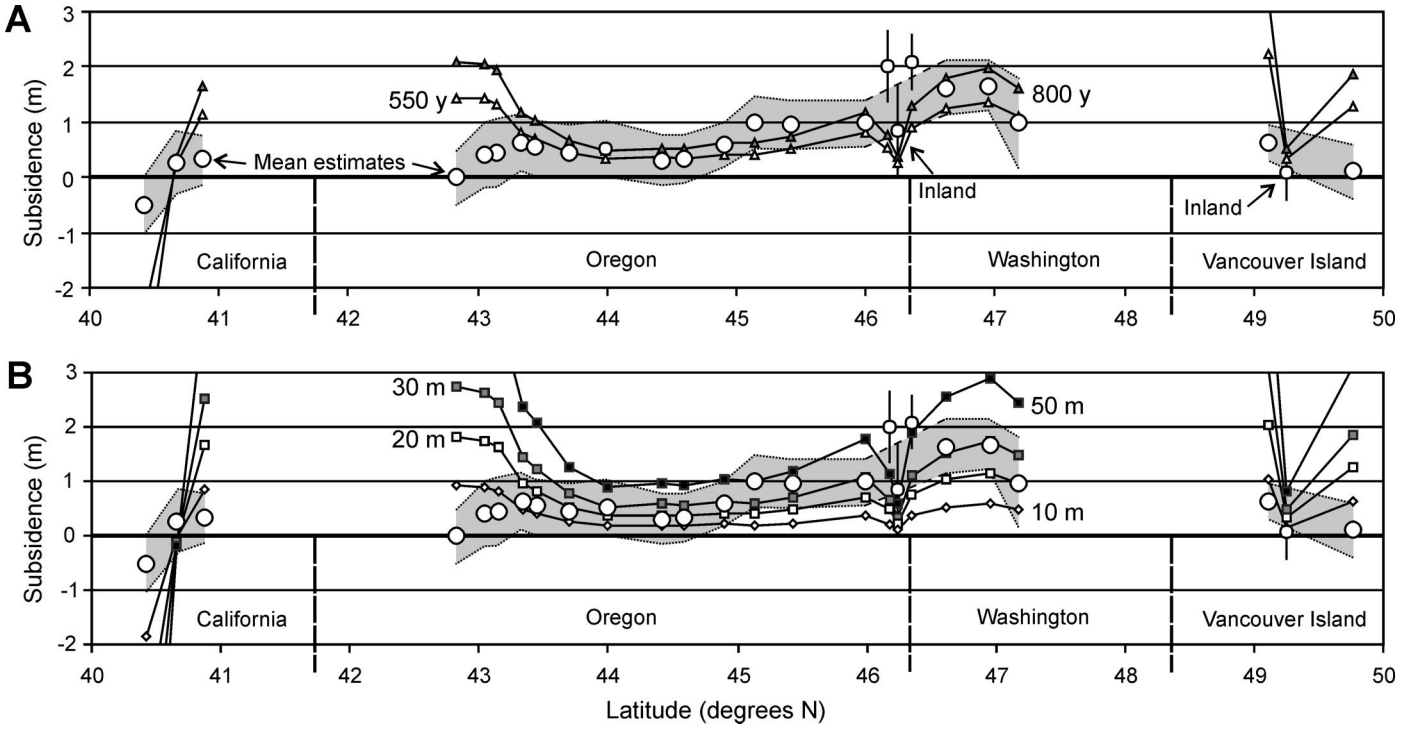

Figure 9. Mean subsidence estimates (from Fig. 6) at averaged locations (see Fig. 10), compared with predictions of elastic dislocation models for same sites. Mean estimates are weighted mean (circles) plus or minus weighted standard deviation (shading) of subsidence estimated at closely spaced sites (Columbia River and Port Alberni data are excluded from shading). Model predicts subsidence expected (A) after 800 and 550 yr of plate convergence; (B) for uniform slip on megathrust of 10, 20, 30, and 50 m.

for 550 yr there is 14.9 m slip in the south increasing to 24.8 m in the north. Model coseismic subsidence is calculated for each of the coastal marsh sites. Figure 9A compares the model coseismic subsidence predictions and the marsh estimates.

The second approach uses models with a constant slip magnitude along the margin but allows for the varying direction of slip along the margin. The predictions for 10, 20, 30, and 50 m slip on the megathrust (and corresponding transition) are shown against latitude in Figure 9B in comparison with the coseismic subsidence estimates obtained through coastal marsh studies. The marsh estimates are the weighted mean and standard deviation of groups of points that are close in latitude and longitude. The results of all models are also shown, plotted against longitude, in comparison with the marsh estimates in Figure 7.

The coastal marsh data are better fit by the models with full release of the strain built up over 550 and 800 yr, respectively (see also Fig. 10 for map view of contoured subsidence predicted after 800 yr). This agreement supports the conclusion that the convergence varies in rate and direction along the margin. The 550- and 800-yr models both produce a similar reasonable agreement with the observed north-south trend of coastal subsidence, fitting within the error of the coastal estimates for much of the margin between south-central Oregon and central Washington. Model time intervals of much less than 550 or greater than 800 yr do not provide satisfactory agreement. None of the models provides a good fit at either end of the subduction zone.

In the south, misfit may be due to breakup of the Gorda Plate and complex subduction tectonics near the Mendocino Triple Junction (e.g., Chaytor et al., 2002). A greater frequency of events implied from the seafloor turbidite record (Goldfinger et al., 1999, 2003) results in a smaller coseismic displacement per event. Displacement on upper plate structures, probably synchronous with megathrust dislocation, may be responsible for the subsidence experienced at some sites in southern Oregon and northern California (e.g., Carver and Burke, 1989; Goldfinger et al., 1992). Our study cannot resolve the relative contributions of the two sources of subsidence; however, we note that the fit between the dislocation model predictions and the subsidence data would be improved in southern Oregon with a narrower locked zone in that area. A narrower locked zone would cause a seaward shift in the model profiles shown in Figure 7.

At the northern, Vancouver Island end of the subduction zone, coseismic subsidence is significantly over-predicted, indicating that the model is a poor representation there. According to uniform slip models, the estimated 1700 coastal subsidence results from less than 10 m of slip on the megathrust. Recent geodetic measurements indicate interseismic uplift rates of ~3 mm/yr on western Vancouver Island (2.6 ± 0.6 from repeated leveling, after Dragert et al. [1994]; 3.8 ± 2 from absolute gravity measurements, Lambert et al. [2001]). This rate is consistent with the average rate for the last 300 yr (Fig. 10). If this uplift rate had been sustained over the ~800 yr since the previous event, one would expect ~2.4 m of subsidence, approximately the same as predicted by the simple dislocation model but significantly greater than the 0.65 m observed (Hughes et al., 2002). If the 0.65 m of subsidence in 1700 represented release of all of the interseismic strain since the previous earthquake, an average interseismic uplift rate of only 0.8 mm/yr over 800 yr is implied. An additional complexity in this area is the lack of buried soils older than the 1700 event on western Vancouver Island, in contrast to the rest of the subduction zone. This absence suggests that there is long-term coastal uplift at a

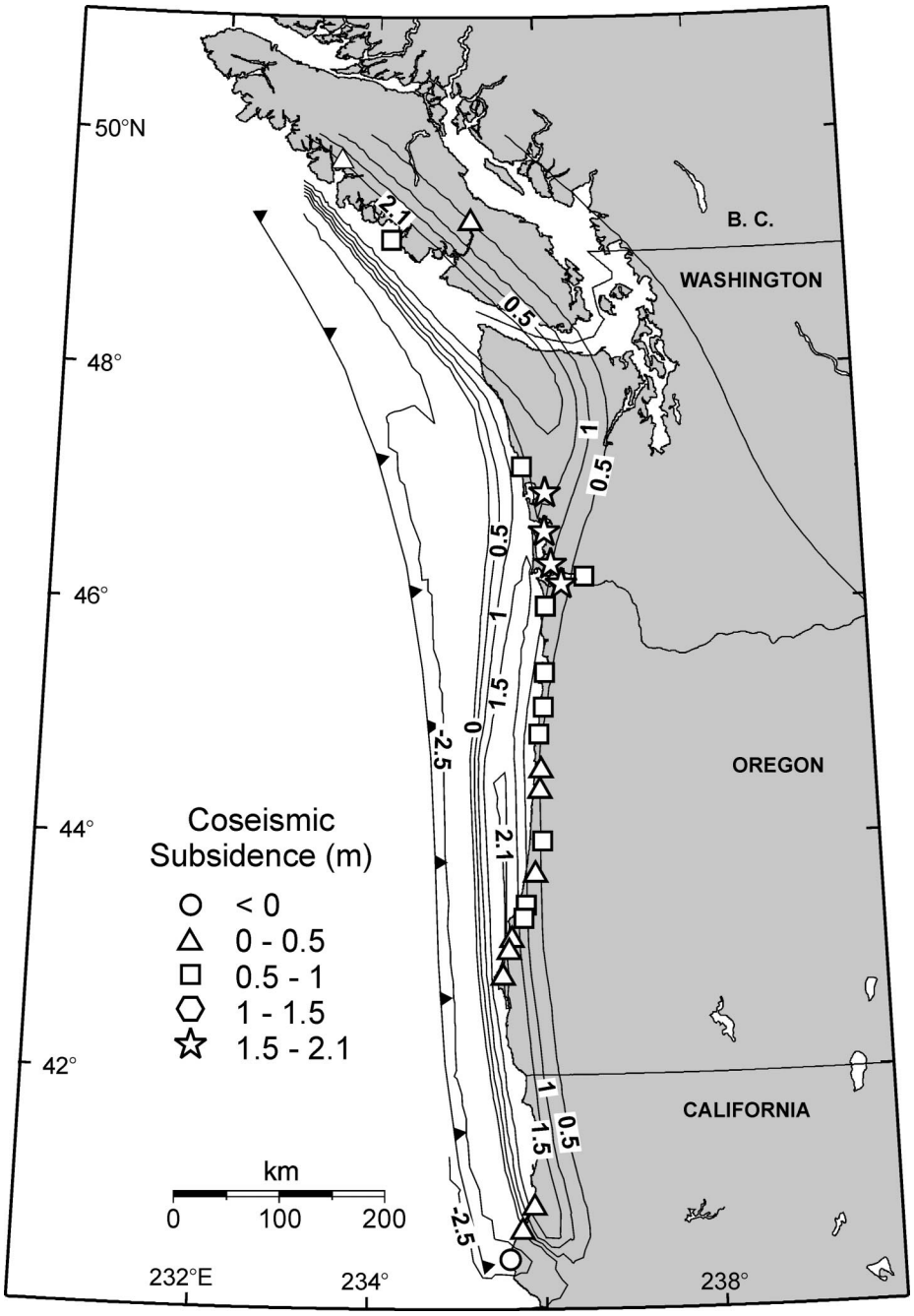

Figure 10. Mean subsidence estimates (symbols) of Figure 6 in comparison with predictions of simple elastic dislocation model (contoured) for elastic release of 800 yr of strain accumulation (Fig. 9A).

rate faster than the sea level rise of ~1.8 mm/yr. Postglacial rebound after retreat of the southern Cordilleran ice sheet can only account for approximately one-third of this long-term uplift (estimated at ~0.55 mm/yr on western Vancouver Island; Fig. 13C *in* Clague and James [2002]). It is possible that the 1700 event released only some fraction of the strain accumulated over the previous ~800 yr and that future earthquakes will cause greater subsidence, that is, the interseismic and coseismic deformation will balance out over a number of earthquake cycles.

Comparisons of the results of uniform slip modeling with subsidence estimates can provide estimates of the magnitude of slip that occurred at different parts of the margin. We have used a simple visual comparison to assign a best-fit uniform slip model for each part of the margin (Fig. 11). Our results indicate a surprisingly smooth variation of rupture slip along the margin in 1700, but some variability among great earthquakes is expected. The dislocation model suggests that the greatest slip in 1700 occurred in northern Oregon/southern Washington (30–50 m), and that slip decreased to the north and south to less than 10 m. Slip along most of the margin is consistent with the expected maximum slip in an M 9 earthquake of ~20–30 m (20–25 m, 1964 Alaska, Johnson et al. [1996]; 20–40 m, 1960 Chile, Barrientos and Ward [1990]; average slip was ~10 m in both events). These slip values indicate a seismic moment release (Brune, 1968) of $\sim 5.6 \times 10^{29}$ to 7×10^{29} N-m, corresponding to a moment magnitude (Hanks and Kanamori, 1979) of 9.1 to 9.2, depending on the tapering of slip toward the ends of the subduction zone. Our result is in agreement with the 1700 event of M 9 suggested from Japanese tsunami wave heights, which require rupture of almost the entire length of the subduction zone (Satake et al., 1996).

The main model anomaly is the Columbia River area, where slip of at least 50 m is suggested. Either this is evidence for significant postseismic creep on the seismogenic fault, or there are problems with the subsidence data. The subsidence data from the more inland Columbia River sites may be biased. Fully saline marine conditions extend only as far upstream as river mile 7 (11.3 km); beyond mile 23 (37 km) the river is fully freshwater (e.g., Pruter and Alverson, 1972). In less saline conditions the elevation zoning relationship may break down; for example, plants usually restricted to higher elevations due to saltwater intolerance may be found at lower elevations.

METHOD 2: ESTIMATING COSEISMIC SUBSIDENCE USING 1700 HORIZON DEPTH

A second method of estimating coseismic subsidence is illustrated in Figure 12, which also shows how interseismic uplift can be deduced (discussed below). The subsurface depth of the buried soil is measured relative to the current marsh elevation, and this figure is corrected for other processes that have affected its vertical position since the 1700 event. These processes include postglacial rebound, eustatic sea-level change, and interseismic uplift (e.g., Hyndman and Wang, 1995). Postglacial rebound is most significant at the northern end of the subduction zone (up to ~0.55 mm/yr) and decreases southward to

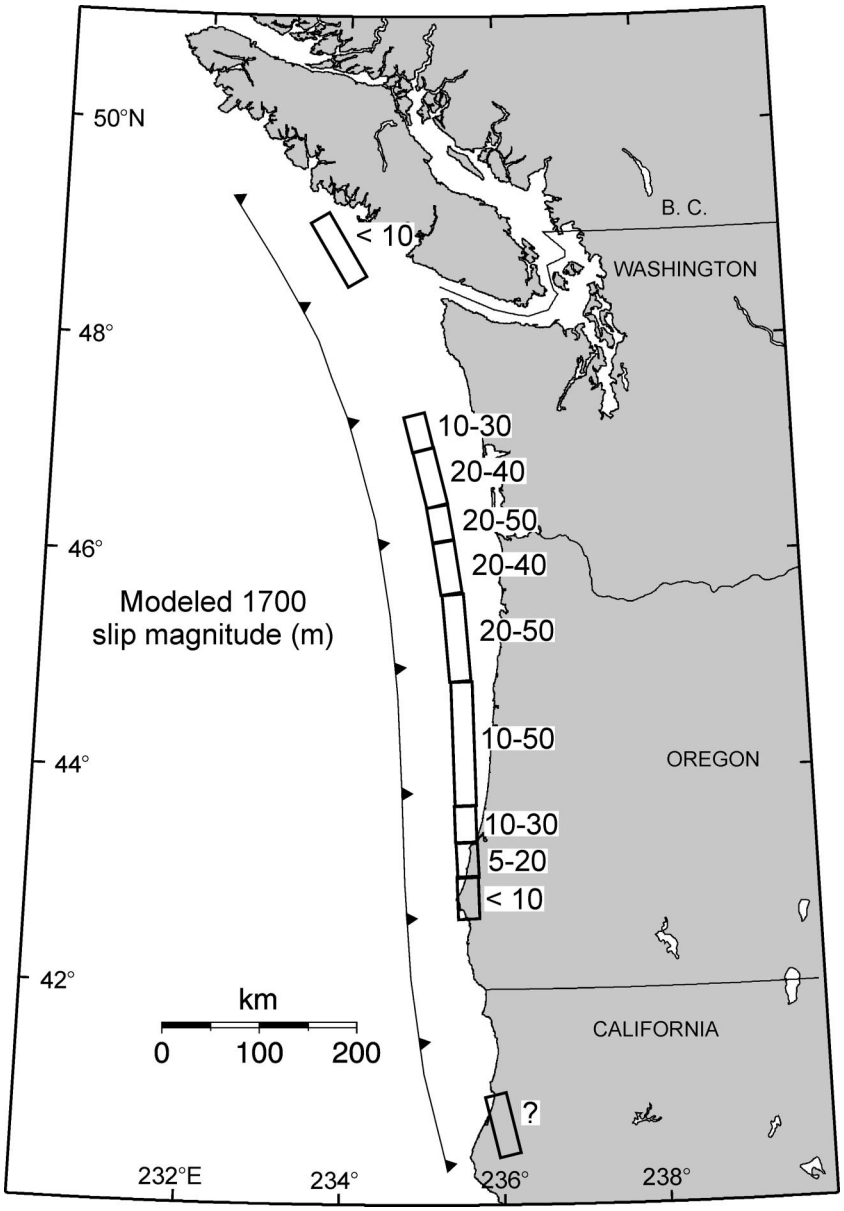

Figure 11. Along-coast variations in slip magnitude for 1700 earthquake, from comparisons of predictions of elastic dislocation uniform slip models with geological subsidence estimates (Fig. 9B). Plate convergence over 800 yr ranges, north to south, from 22 to 36 m.

zero by ~45°N at the coast (Fig. 13C *in* Clague and James, 2002); corrections of 0 to + 0.55 mm/yr are accordingly applied to the depth data for the northern half of the subduction zone. Eustatic sea level has risen by ~1.8 mm/yr over the last 100 yr (Douglas, 1991); a correction of −1.8 mm/yr for every year from 1700 to the year of measurement is applied.

Total interseismic uplift is more difficult to quantify. In this study we use an elastic dislocation model (constrained mainly by leveling and tide gauge data and using current convergence directions and rates) to predict the interseismic uplift at each site. The convergence rate between the Juan de Fuca plate and the Cascadia forearc is based on recent (~1 m.y.) plate motion models and integrates separate Explorer, Gorda, and Oregon forearc micro-blocks (cf. Mazzotti et al., 2002, for a description). The resultant interseismic uplift correction, and therefore the subsidence estimates (Fig. 13), is dependent on the details of the input fault slip geometry, that is, whether one uses the transition zone with linear downdip slip decay of Flück et al. (1997) or the larger ''effective'' transition zone with exponential downdip decay of Wang et al. (2003).

This method for estimating coseismic subsidence assumes that sediment supply has kept pace with the available vertical accommodation and that the sediments at the modern surface lie at an elevation equal to the paleoelevation of the pre-earthquake surface, that is, that the modern and 1700 marsh surfaces at a particular site formed in the same intertidal zone.

As the true geometry of the coseismic and interseismic transition zone remains uncertain, estimates of coseismic subsidence gained using this method are far from robust. However, the pattern of coseismic subsidence is broadly similar to that obtained from coastal marsh studies that use elevation indicators (Fig. 6) and thus provides support for the latter estimates.

An alternative way to use the marsh burial depth is to fix the subsidence using estimates derived from the paleoelevation method (Figs. 6 and 7) and calculate the total interseismic uplift since 1700 (Fig. 14). When converted to millimeters per year, the resultant uplift rates (triangles) generally compare well with current geodetically determined uplift rates (circles and shading; Hyndman and Wang, 1995) in the central and northern subduction zone. This implies that current uplift rates (midway through the average earthquake cycle) are about the same as the average uplift rate throughout this earthquake cycle so far. In the southern portion, calculated uplift is lower than current measurements and appears to be more comparable to long-term (~100 k.y.) rates determined from uplifted shore platforms (squares; Kelsey et al., 1994). Goldfinger et al. (1999) found more frequent events in seafloor turbidite sequences of the southern end of the Cascadia subduction zone, probably due to breakup of the Gorda Plate as mentioned above. Thus, 1700 slip at the southern end was likely smaller than elsewhere.

CONCLUSIONS

Coseismic subsidence in the 1700 great Cascadia earthquake, as estimated from marsh paleoelevation studies, is approximately equal to that predicted by elastic dislocation models constrained by interseismic geodetic data and thermal models. The uncertainties in paleoelevation estimates of coseismic subsidence are large, but there is a clear and consistent pattern along the margin. Greatest coseismic subsidence (~1–2 m) occurred in northern

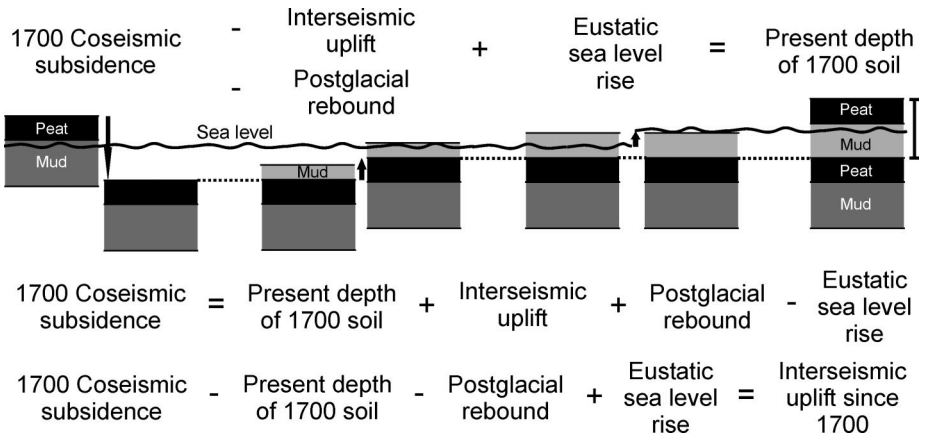

Figure 12. Method 2: Method for estimating coseismic subsidence using depth of 1700 peat horizon below modern marsh top (results in Fig. 13). Also shown is an independent method of estimating interseismic uplift since 1700, using marsh coseismic subsidence estimates, depth of 1700 horizon, postglacial rebound, and eustatic sea-level rise (results in Fig. 14).

Oregon/southern Washington; other areas appear to have subsided between 0 and 1 m in the earthquake, with coseismic uplift experienced at part of the southernmost end of the subduction zone. The predictions of the models are in broad agreement with the marsh subsidence estimates, the best-fitting models being those that simulate the elastic release of 550–800 yr of strain accumulation at the plate convergence rate.

The comparison of uniform slip model predictions with marsh coseismic subsidence estimates allows the estimation of slip magnitude in the 1700 earthquake. The best-fit slip pattern (Fig. 11) shows a region of large and nearly constant coseismic/tsunamigenic slip; greatest slip is indicated in northern Oregon/southern Washington (≥ 30 m), declining along the coast to the north and south to less than 10 m. Fault rupture of 10–30 or even

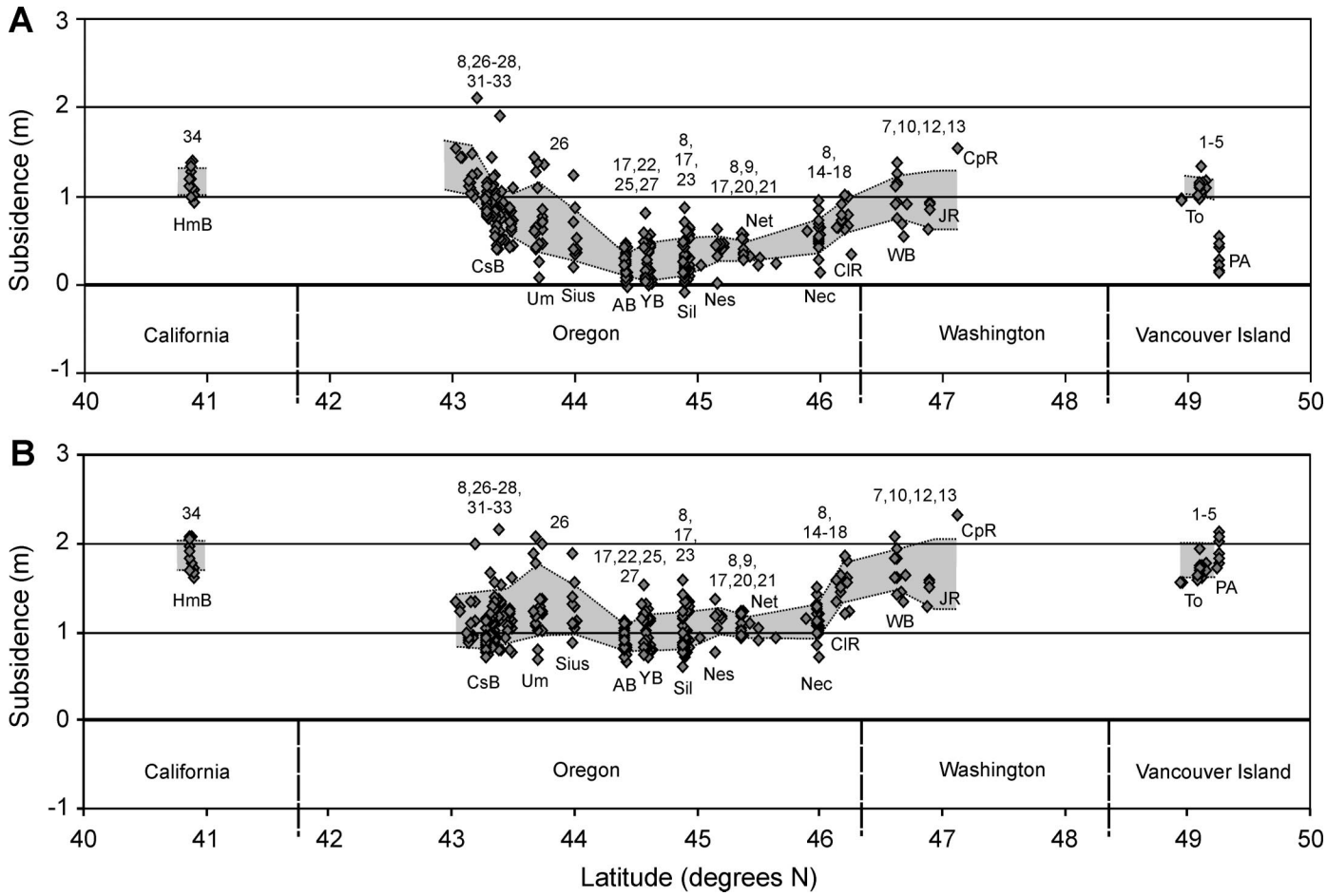

Figure 13. Compilation of coseismic subsidence estimates made using method described in Figure 12 (method 2). Measurements of depth of buried soil were corrected for eustatic sea-level rise (assumed constant at 1.8 mm/yr), postglacial rebound, and interseismic uplift, (A) using elastic dislocation model of Flück et al., 1997, (B) using revised dislocation model of Wang et al. (2003). Gray shading represents mean plus or minus standard deviation of groups of points. Locations and abbreviations are shown in Figure 4. Numbers above data points reference data sources (see Table 1).

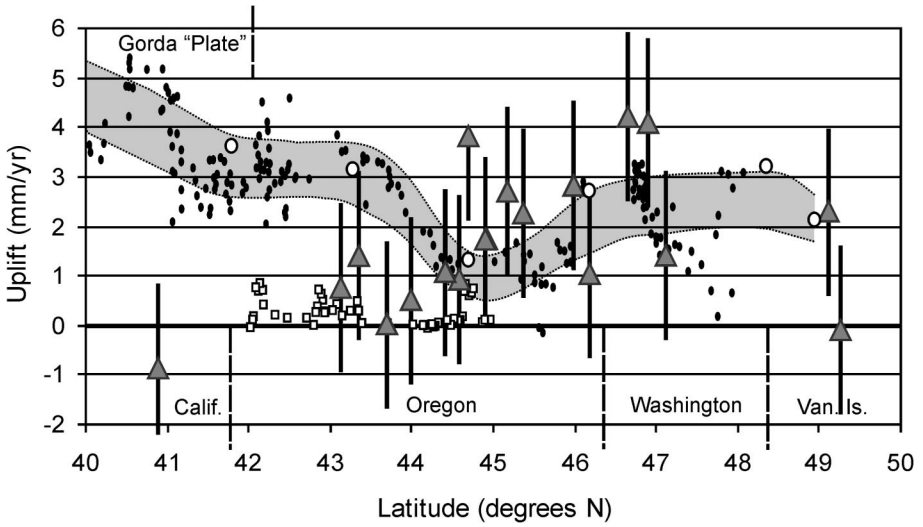

Figure 14. Interseismic uplift since 1700 (gray triangles) calculated inversely using method shown in Figure 12 (method 2) and converted to millimeters per year, compared with recent geodetic measurements of uplift (open circles, tide gauge data; filled circles, leveling data; shaded curve represents ~1σ of geodetic data; Hyndman and Wang, 1995) and long-term uplift estimates based on uplifted shore platforms of 80, 105, and 125 ka (open squares; Kelsey et al., 1994). Error bars are based on assumed error of subsidence estimates of ± 0.5 m. Calif.—California; Van. Is.—Vancouver Island.

40 m is consistent with the M 9 earthquake indicated by Japanese tsunami records.

Discrepancies exist, however, at the southern and northern ends of the subduction zone. In the south, misfit may be due to breakup of the Gorda plate, resulting in a greater number of events of smaller magnitude. In southern Oregon, a better fit would be achieved with a somewhat narrower locked zone. In the north, the paleoelevation subsidence estimates are three to four times smaller than is predicted by the release of the model interseismic strain accumulated since the previous event (~800 yr). The model interseismic uplift is consistent with the average uplift since 1700. The discrepancy may be explained if the 1700 event released only part of the accumulated strain at the northern end of the subduction zone; this idea is consistent with the greater net uplift experienced, which is evidenced by the lack of buried soils older than 1700, in contrast to the rest of the subduction zone.

Average uplift rates since 1700, estimated from the depth of the 1700 marsh-top horizon, paleoelevation subsidence estimates, postglacial rebound, and eustatic sea-level rise, agree with current geodetically determined uplift rates for the central and northern portions of the subduction zone. In the south, however, the small uplift calculated via this method is more comparable to long-term (~100 k.y.) uplift rates determined from uplifted shore platforms, again perhaps reflecting internal deformation of the Gorda plate.

ACKNOWLEDGMENTS

Reviews by David Eaton, Curt Peterson, and Anne Trehu significantly improved the manuscript. We acknowledge helpful discussions with Brian Atwater, John Clague, Kelin Wang, Tom James, Joe English, Rob Witter, and Herb Dragert. All maps were prepared using GMT software (Wessel and Smith, 1995). Financial support is acknowledged from a University of Victoria graduate fellowship, the Natural Sciences and Engineering Research Council, the U.S. Geological Survey National Earthquake Hazards Reduction Program External Research Program, and External Research Program, and facilities and research support from the Geological Survey of Canada. This contribution is Geological Survey of Canada publication 2002281.

REFERENCES CITED

Adams, J., 1990, Paleoseismicity of the Cascadia subduction zone: Evidence from turbidites off the Oregon-Washington margin: Tectonics, v. 9, p. 569–583.

Atwater, B.F., 1987, Evidence for great Holocene earthquakes along the outer coast of Washington State: Science, v. 336, p. 942–944.

Atwater, B.F., 1988, Geologic studies for seismic zonation of the Puget lowland, *in* Jacobson, M.L., and Rodriguez, T.R., compilers, National Earthquake Hazards Reduction Program, Summaries of technical reports, Volume 25: U.S. Geological Survey Open-File Report 88–16, p. 120–133.

Atwater, B.F., 1992, Geologic evidence for earthquakes during the past 2000 years along the Copalis River, southern coastal Washington: Journal of Geophysical Research, v. 97, p. 1901–1919.

Atwater, B.F., 1994, Geology of Holocene liquefaction features along the lower Columbia River at Marsh, Brush, Hunting, and Wallace Islands, Oregon and Washington: U.S. Geological Survey Open File Report 94–209, 63 p.

Atwater, B.F., and Hemphill-Haley, E., 1997, Recurrence intervals for great earthquakes of the past 3,500 years at northeastern Willapa Bay, Washington: U.S. Geological Survey Professional Paper 1576, 108 p.

Atwater, B.F., Nelson, A.R., Clague, J.J., Carver, G.A., Yamaguchi, D.K., Bobrowsky, P.T., Bourgeois, J., Darienzo, M.E., Grant, W.C., Hemphill-Haley, E., Kelsey, H.M., Jacoby, G.C., Nishenko, S.P., Palmer, S.P., Peterson, C.D., and Reinhart, M.A., 1995, Summary of coastal geologic evidence for past great earthquakes at the Cascadia subduction zone: Earthquake Spectra, v. 11, p. 1–18.

Atwater, B.F., Yamaguchi, D.K., Bondevik, S., Barnhardt, W.A., Amidon, L.J., Benson, B.E., Skjerdal, G., Shulene, J.A., and Nanayama, F., 2001, Rapid resetting of an estuarine recorder of the 1964 Alaska earthquake: Geological Society of America Bulletin, v. 113, p. 1193–1204.

Barrientos, S.E., and Ward, S.N., 1990, The 1960 Chile earthquake: Inversion for slip distribution from surface deformation: Geophysical Journal International, v. 103, p. 589–598.

Barnett, E.T., 1997, The potential for coastal flooding due to coseismic subsidence in the central Cascadia margin [M.S. thesis]: Portland State University, Portland, Oregon, 144 p.

Briggs, G.G., 1994, Coastal crossing of the zero-isobase, Cascadia margin, south-central Oregon coast [M.S. thesis]: Portland State University, Portland, Oregon, 251 p.

Briggs, G., and Peterson, C.D., 1993, Neotectonics of the central Cascadia margin as recorded on south-central Oregon coastal deposits: Washington, D.C., U.S. Geological Survey—National Earthquake Hazards Reduction Program Final Report, 77 p.

Brown, L.D., Reilinger, R.E., Holdahl, S.R., and Balazs, E.I., 1977, Postseismic crustal uplift near Anchorage, Alaska: Journal of Geophysical Research, v. 82, p. 3369–3378.

Brune, J.N., 1968, Seismic moment, seismicity, and rate of slip along major fault zones: Journal of Geophysical Research, v. 73, p. 777–784.

Carver, G., and Burke, R.B., 1989, Active convergent tectonics in northwestern California, *in* Aalto, K.R., et al., field trip leaders, Geological evolution of the northernmost Coast Ranges and western Klamath Mountains, California, *in* International Geologic Congress, 28th, Field Trip Guidebook T308: Washington, D.C., American Geophysical Union, p. 64–82.

Carver, G., Jayko, A.S., Valentine, D.W., and Li, W.H., 1994, Coastal uplift associated with the 1992 Cape Mendocino earthquake, northern California: Geology, v. 22, p. 195–198.

Chaytor, J.D., Goldfinger, C., and Dziak, R.P., 2002, The structural evolution of the Gorda ''Plate'': Destruction of a plate fragment prior to subduction in the Cascadia subduction zone [abs.]: Eos (Transactions, American Geophysical Union), v. 83, p. F1259.

Clague, J.J., and Bobrowsky, P.T., 1994a, Evidence for a large earthquake and tsunami 100–400 years ago on western Vancouver Island, British Columbia: Quaternary Research, v. 41, p. 176–184.

Clague, J.J., and Bobrowsky, P.T., 1994b, Tsunami deposits in tidal marshes on Vancouver Island, British Columbia: Geological Society of America Bulletin, v. 106, p. 1293–1303.

Clague, J.J., and James, T.S., 2002, History and isostatic effects of the last ice sheet in southern British Columbia: Quaternary Science Reviews, v. 21, p. 71–87.

Combellick, R.A., 1986, Chronology of late-Holocene earthquakes in south central Alaska; evidence from buried organic soils in upper Turnagain Arm:, Geological Society of America Abstracts with Programs, v. 18, no. 6, p. 569.

Darienzo, M.E., 1991, Late Holocene paleoseismicity along the northern Oregon coast [Ph.D. thesis]: Portland State University, Portland, Oregon, 176 p.

Darienzo, M.E., and Peterson, C.D., 1990, Episodic tectonic subsidence of late Holocene salt marshes, northern Oregon central Cascadia margin: Tectonics, v. 9, p. 1–22.

Darienzo, M.E., and Peterson, C.D., 1995, Magnitude and frequency of subduction-zone earthquakes along the northern Oregon coast in the past 3,000 years: Oregon Geology, v. 57, p. 3–12.

Douglas, B.C., 1991, Global sea level rise: Journal of Geophysical Research, v. 96, p. 6981–6992.

Dragert, H., Hyndman, R.D., Rogers, G.C., and Wang, K., 1994, Current deformation and the width of the seismogenic zone of the northern Cascadia subduction thrust: Journal of Geophysical Research, v. 99, p. 653–668.

Flück, P., Hyndman, R.D., and Wang, K, 1997, Three-dimensional dislocation model for great earthquakes of the Cascadia subduction zone: Journal of Geophysical Research, v. 102, p. 20,539–20,550.

Frey, R.W., and Basan, P.B., 1985, Coastal salt marshes, *in* Davis, R.A., Jr., ed., Coastal sedimentary environments: New York, Springer-Verlag, p. 101–169.

Gallaway, P.J., Peterson, C.D., Watkins, A.M., Craig, S., and McLeod, B.L., 1992, Paleotsunami runup at Cannon Beach, Oregon: Clatsop County, Oregon, Final Report to Clatsop County Sheriffs Office, 36 p.

Goldfinger, C., Kulm, L.D., Yeats, R.S., Appelgate, B., MacKay, M.E., and Moore, G.F., 1992, Transverse structural trends along the Oregon convergent margin: Implications for Cascadia earthquake potential and crustal rotations: Geology, v. 20, p. 141–144.

Goldfinger, C., Nelson, H., and Johnson, J.E., 1999, Holocene recurrence of Cascadia great earthquakes based on the turbidite event record [abs.]: Eos (Transactions, American Geophysical Union), v. 80, p. 1024–1025.

Goldfinger, C., Nelson, C.H., Johnson, J.E., and the Shipboard Scientific Party, 2003, Holocene earthquake records from the Cascadia subduction zone and northern San Andreas fault based on precise dating of offshore turbidites: Annual Review of Earth and Planetary Sciences, v. 31, p. 555–577.

Guilbault, J.P., Clague, J.J., and Lapointe, M., 1995, Amount of subsidence during a late Holocene earthquake—Evidence from fossil tidal marsh foraminifera at Vancouver Island, west coast of Canada: Palaeogeography, Palaeoclimatology, Palaeoecology, v. 118, p. 49–71.

Guilbault, J.P., Clague, J.J., and Lapointe, M., 1996, Foraminifera evidence for the amount of coseismic subsidence during a late Holocene earthquake on Vancouver Island, west coast of Canada: Quaternary Science Reviews, v. 15, p. 913–937.

Hanks, T.C., and Kanamori, H., 1979, A moment magnitude scale: Journal of Geophysical Research, v. 84, p. 2348–2350.

Hemphill-Haley, E., 1992, The application of diatom paleoecology to interpretations of Holocene relative sea-level change and coseismic subsidence in southwestern Washington [Ph.D. thesis]: Santa Cruz, University of California, 321 p.

Hemphill-Haley, E., 1995a, Intertidal diatoms from Willapa Bay, Washington: Application to studies of small-scale sea-level changes: Northwest Science, v. 69, p. 29–45.

Hemphill-Haley, E., 1995b, Diatom evidence for earthquake-induced subsidence and tsunami 300 yr ago in southern coastal Washington: Geological Society of America Bulletin, v. 107, p. 367–378.

Hughes, J.F., Mathewes, R.W., and Clague, J.J., 2002, Use of pollen and vascular plants to estimate coseismic subsidence at a tidal marsh near Tofino, British Columbia: Palaeogeography, Palaeoclimatology, Palaeoecology, v. 185, p. 145–161.

Hutchinson, I., Guilbault, J.P., Clague, J.J., and Bobrowsky, P.T., 2000, Tsunamis and tectonic deformation at the northern Cascadia margin; a 3000-year record from Deserted Lake, Vancouver Island, British Columbia, Canada: The Holocene, v. 10, p. 429–439.

Hyndman, R.D., and Wang, K., 1993, Thermal constraints on the zone of major thrust earthquake failure: The Cascadia subduction zone: Journal of Geophysical Research, v. 98, p. 2039–2060.

Hyndman, R.D., and Wang, K., 1995, The rupture zone of Cascadia great earthquakes from current deformation and the thermal regime: Journal of Geophysical Research, v. 100, p. 22,133–22,154.

Jacoby, G.C., Carver, G.A., and Wagner, W., 1995, Trees and herbs killed by an earthquake 300 yr ago at Humboldt Bay, California: Geology, v. 23, p. 77–80.

Jacoby, G.C., Bunker, D.E., and Benson, B.E., 1997, Tree-ring evidence for an A.D. 1700 Cascadia earthquake in Washington and northern Oregon: Geology, v. 25, p. 999–1002.

Jennings, A.E., and Nelson, A.R., 1992, Foraminiferal assemblage zones in Oregon tidal marshes: Relation to marsh floral zones and sea level: Journal of Foraminiferal Research, v. 22, p. 13–29.

Johnson, J.M., Satake, K., Holdahl, S.R., and Sauber, J., 1996, The 1964 Prince William Sound earthquake: Joint inversion of tsunami and geodetic data: Journal of Geophysical Research, v. 101, p. 523–532.

Kelsey, H.M., Engebretson, D.C., Mitchell, C.E., and Ticknor, R.L., 1994, Topographic form of the coast ranges of the Cascadia margin in relation to coastal uplift rates and plate subduction: Journal of Geophysical Research, v. 99, p. 12,245–12,255.

Lambert, A., Courtier, N., Dragert., H., James, T.S., Schmidt, M., Wang, K., and He, J., 2001, Absolute gravity measurements in the Cascadia Subduction Zone [abs.]: Eos (Transactions, American Geophysical Union), v. 82, p. F285.

Li, W.H., 1992, Late Holocene paleoseismology in the lower Eel River valley, northern California [M.S. thesis]: Arcata, California, Humboldt State University, 78 p.

Long, A.J., and Shennan, I., 1998, Models of rapid relative sea-level change in Washington and Oregon, USA: The Holocene, v. 8, p. 129–142.

Ludwin, R.S., 2002, Cascadia megathrust earthquakes in Pacific Northwest Indian myths and legends: TsuInfo Alert, National Tsunami Hazard Mitigation Program, v. 4, no. 2, p. 6–10.

Mazzotti, S., Dragert, H., Hyndman, R.D., Miller, M.M., and Henton, J.A., 2002, GPS deformation in a region of high crustal seismicity: N. Cascadia forearc: Earth and Planetary Science Letters, v. 198, p. 41–48.

McCaffrey, R., Long, M.D., Goldfinger, C., Zwick, P.C., Nabelek, J.L., Johnson, C.K., and Smith, C., 2000, Rotation and plate locking at the southern Cascadia subduction zone: Geophysical Research Letters, v. 27, p. 3117–3120.

Merritts, D.J., 1996, The Mendocino triple junction: Active faults, episodic coastal emergence, and rapid uplift: Journal of Geophysical Research, v. 101, p. 6051–6070.

Miller, M.M., Johnson, D.J., Rubin, C.M., Dragert, H., Wang, K., Qamar, A., and Goldfinger, C., 2001, GPS-determination of along-strike variation in Cascadia margin kinematics; implications for relative plate motion, subduction zone coupling, and permanent deformation: Tectonics, v. 20, p. 161–176.

Mitchell, C.E., Vincent, P., Weldon, R.J., II, and Richards, M.A., 1994, Present-day vertical deformation of the Cascadia margin, Pacific Northwest, USA: Journal of Geophysical Research, v. 99, p. 12,257–12,277.

Nelson, A.R., 1992, Holocene tidal-marsh stratigraphy in south-central Oregon–Evidence for localized sudden submergence in the Cascadia subduction zone, *in* Fletcher, C.H., III, et al., eds., Quaternary coasts of the United States: Marine and lacustrine systems: SEPM (Society for Sedimentary Geology) Special Publication 48, p. 287–301.

Nelson, A.R., and Kashima, K., 1993, Diatom zonation in southern Oregon tidal marshes relative to vascular plants, foraminifera, and sea level: Journal of Coastal Research, v. 9, p. 673–697.

Nelson, A.R., Shennan, I., and Long, A.J., 1996a, Identifying coseismic subsidence in tidal-wetland stratigraphic sequences at the Cascadia subduction zone of western North America: Journal of Geophysical Research, v. 101, p. 6115–6135.

Nelson, A.R., Jennings, A.E., and Kashima, K., 1996b, An earthquake history derived from stratigraphic and microfossil evidence of relative sea-level change at Coos Bay, southern coastal Oregon: Geological Society of America Bulletin, v. 108, p. 141–154.

Nelson, A.R., Ota, Y., Umitsu, M., Kashima, K., and Matsushima, Y., 1998, Seismic or hydrodynamic control of rapid late-Holocene sea-level rises in southern coastal Oregon, USA?: The Holocene, v. 8, p. 287–299.

Okada, Y., 1985, Surface deformation due to shear and tensile faults in a half-space: Seismological Society of America Bulletin, v. 75, p. 1135–1154.

Ovenshine, A.T., Lawson, D.E., and Bartsch-Winkler, S.R., 1976, The Placer River Silt—An intertidal deposit caused by the 1964 Alaska earthquake: U.S. Geological Survey Journal of Research, v. 4, p. 151–162.

Peterson, C.D., and Darienzo, M.E., 1988, Coastal neotectonic field trip guide for Netarts Bay, Oregon: Oregon Geology, v. 50, no. 9/10, p. 99–106, and 117.

Peterson, C.D., and Darienzo, M.E., 1989, Episodic, abrupt tectonic subsidence recorded in late Holocene deposits of the South Slough syncline: An on-land expression of shelf fold belt deformation from the southern Cascadia margin: Geological Society of America Abstracts with Programs, v. 21, no. 5, p. 129.

Peterson, C.D., and Darienzo, M.E., 1991, Discrimination of climatic, oceanic and tectonic mechanisms of cyclic marsh burial from Alsea Bay, Oregon, USA: U.S. Geological Survey Open File Report 91–441-C, 53 p.

Peterson, C.D., and Darienzo, M.E., 1996, Discrimination of flood, storm and tectonic subsidence events in coastal marsh records of Alsea Bay, central Cascadia margin, USA, *in* Rogers, A.M., et al., eds., Assessing earthquake hazards and reducing risk in the Pacific Northwest, Volume 1: U.S. Geological Survey Professional Paper 1560, p. 115–146.

Peterson, C.D., and Madin, I.P., 1997, Coseismic paleoliquefaction evidence in the central Cascadia margin, USA: Oregon Geology, v. 59, p. 51–74.

Peterson, C.D., and Priest, G.R., 1995, Preliminary reconnaissance of Cascadia paleotsunami deposits in Yaquina Bay, Oregon: Oregon Geology, v. 57, p. 33–40.

Peterson, C.D., Darienzo, M.E., Burns, S.F., and Burris, W., 1993, Field trip guide to Cascadia paleoseismic evidence along the northern Oregon coast: Evidence of subduction zone paleoseismicity in the central Cascadia margin: Oregon Geology, v. 55, p. 99–114.

Peterson, C.D., Darienzo, M.E., Doyle, D., and Barnett, E., 1996, Evidence for coseismic subsidence and tsunami deposition during the past 3,000 years at Siletz Bay, Oregon, *in* Priest, G.R., ed., Explanation of mapping methods and use of the tsunami hazard map of the Siletz Bay area, Lincoln City, Oregon: Oregon Department of Geology and Mineral Industries Open File Report 0–95–5, 25 p.

Peterson, C.D., Barnett, E.T., Briggs, G.C., Carver, G.A., Clague, J.J., and Darienzo, M.E., 1997, Estimates of coastal subsidence from great earthquakes in the Cascadia subduction zone, Vancouver Island, B.C., Washington, Oregon, and northernmost California: State of Oregon Department of Geology and Mineral Industries Open File Report, 44 p.

Peterson, C.D., Doyle, D.L., and Barnett, E.T., 2000, Coastal flooding and beach retreat from coseismic subsidence in the central Cascadia margin, USA: Environmental and Engineering Geoscience, v. 6, p. 255–269.

Plafker, G., 1972, Alaskan earthquake of 1964 and Chilean earthquake of 1960: Implications for arc tectonics: Journal of Geophysical Research, v. 77, p. 901–925.

Plafker, G., and Savage, J.C., 1970, Mechanism of the Chilean earthquakes of May 21 and 22, 1960: Geological Society of America Bulletin, v. 81, p. 1001–1030.

Pruter, A.T., and Alverson, D.L., eds., 1972, The Columbia River estuary and adjacent waters: Bioenvironmental studies: Seattle, University of Washington Press, 868 p.

Satake, K., Shimazaki, K., Tsuji, Y., and Ueda, K., 1996, Time and size of a giant earthquake in Cascadia inferred from Japanese tsunami records of January 1700: Nature, v. 379, p. 246–249.

Savage, J.C., and Lisowski, M., 1991, Strain measurements and the potential for a great subduction earthquake off the coast of Washington: Science, v. 252, p. 101–103.

Savage, J.C., and Thatcher, W., 1992, Interseismic defor-

mation at the Nankai Trough, Japan: Journal of Geophysical Research, v. 97, p. 11,117–11,135.
Scott, D.B., and Medioli, F.S., 1980, Quantitative studies of marsh foraminiferal distributions in Nova Scotia: Implications for sea level studies: Cushman Foundation for Foraminiferal Research, v. 10, p. 205–234.
Shennan, I., Long, A.J., Rutherford, M.M., Green, F.M., Innes, J.B., Lloyd, J.M., Zong, Y., and Walker, K.J., 1996, Tidal marsh stratigraphy, sea-level change and large earthquakes, I: A 5000 year record in Washington, USA: Quaternary Science Reviews, v. 15, p. 1023–1059.
Shennan, I., Long, A.J., Rutherford, M.M., Innes, J.B., Green, F.M., and Walker, K.J., 1998, Tidal marsh stratigraphy, sea-level change and large earthquakes; II: submergence events during the last 3500 years at Netarts Bay, Oregon, USA: Quaternary Science Reviews, v. 17, p. 365–393.
Svarc, J.L., Savage, J.C., Prescott, W.H., and Murray, M.H., 2002, Strain accumulation and rotation in western Oregon and southwestern Washington: Journal of Geophysical Research, v. 107, doi: 10.1029/2001JB000625.
Thatcher, W., 1984, The earthquake deformation cycle at the Nankai Trough, Japan: Journal of Geophysical Research, v. 89, p. 3087–3101.
Vick, G.S., 1988, Late Holocene paleoseismicity and relative sea level changes of the Mad River Slough, northern Humboldt Bay, California [M.S. thesis]: Arcata, California, Humboldt State University, 87 p.
Wang, K., Wells, R., Mazzotti, S., Hyndman, R.D., and Sagaya, T., 2003, A revised dislocation model of interseismic deformation of the Cascadia subduction zone: Journal of Geophysical Research, v. 108, p. 2026.
Wessel, P., and Smith, W.H.F., 1995, New version of the Generic Mapping Tools released [abs.]: Eos (Transactions, American Geophysical Union), v. 76, p. F329.
Wilson, D.S., 1993, Confidence intervals for motion and deformation of the Juan de Fuca plate: Journal of Geophysical Research, v. 98, p. 16,053–16,071.
Witter, R.C., Kelsey, H.M., and Hemphill-Haley, E., 1997, A paleoseismic history of the south-central Cascadia subduction zone; assessing earthquake recurrence intervals and upper-plate deformation over the past 6600 years at the Coquille River estuary, southern Oregon, U.S.A.: U.S. Geological Survey National Earthquake Hazards Reduction Program External Research Program Final Technical Report, Award G3036, 54 p.
Wright, C., and Mella, A., 1963, Modifications to the soil pattern of south-central Chile resulting from seismic and associated phenomena during the period May to August 1960: Bulletin of the Seismological Society of America, v. 53, p. 1367–1402.
Yamaguchi, D.K., Atwater, B.F., Bunker, D.E., Benson, B.E., and Reid, M.S., 1997, Tree-ring dating the 1700 Cascadia earthquake: Nature, v. 389, p. 922–923.

Manuscript Received by the Society 28 March 2003
Revised Manuscript Received 30 July 2003
Manuscript Accepted 10 September 2003

Printed in the USA